

# Supramolecular Interaction Controlled Diffusion Mechanism and Improved Mechanical Behavior of Hybrid Hydrogel Systems of Zwitterions and CNT

Saud Hashmi,<sup>‡</sup> Amin GhavamiNejad,<sup>†</sup> Francis O. Obiweluzor,<sup>†</sup> Mohammad Vatankeh-Varnoosfaderani,<sup>\*,§</sup> and Florian J. Stadler<sup>\*,†</sup>

<sup>†</sup>School of Semiconductor and Chemical Engineering, Chonbuk National University, Baekjero 567, Deokjin-gu, Jeonju, Jeonbuk, 561-756, Republic of Korea

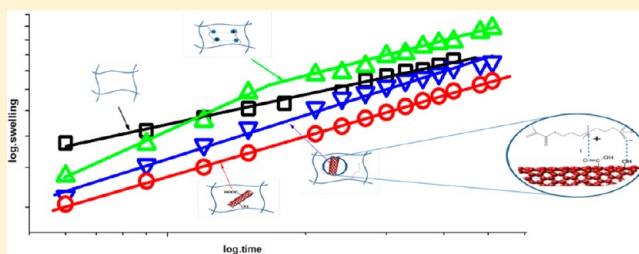
<sup>‡</sup>Department of Chemical Engineering, NED University of Engineering & Technology, University Road, Karachi-75270, Pakistan

<sup>§</sup>Department of Polymer Engineering, Amirkabir University of Technology, 424 Hafez Ave, P.O. Box 15875-4413, Tehran, Iran

## Supporting Information

**ABSTRACT:** Hybrid hydrogels of poly(*N*-isopropylacrylamide) (pNIPAM) containing carboxylate carbon nanotubes (CNTs) and/or zwitterions are synthesized by free radical polymerization. The supramolecular interactions among zwitterionic monomers and CNTs influence the mechanical properties and diffusion mechanism in hybrid hydrogel systems. These supramolecular interactions and response behavior of hybrid hydrogels were tested mechanically and with respect to their swelling characteristics. Hybrid hydrogels of pNIPAM and CNT or pNIPAM, zwitterions, and CNT

follow a Fickian diffusion behavior, while adding zwitterions leads to an anomalous triple-stage swelling behavior and stiffening of the gel due to the interactions of the zwitterions with each other, which significantly increase the viscous dissipation and change the microscopic structure. While CNT itself stiffens the gel and slightly increases the diffusion speed, it complexes zwitterions, which leads to a novel property profile that is both potentially antibiotic and electrically conductive. CNT affords a relaxation process at long relaxation times, while zwitterion attachment and detachment lead to dissipation predominantly at high frequencies. Dynamic rheological measurements were performed during swelling of these complex materials.



## INTRODUCTION

Carbon nanotubes (CNTs) are considered to be an ideal candidate for the manufacture of the next generation of composite materials. In the past 10 years, research on the application of CNTs was performed intensively due to their unique mechanical and electrical properties. In order to harvest the full potential of the CNT–polymer composites, researchers have focused on attaching functional groups to the nanotube surface.

Since CNTs were successfully solubilized in organic solvents<sup>1</sup> and in aqueous solution,<sup>2</sup> their application in the biological field has gained increasing attention. Their unique mechanical, optical, and electrical properties<sup>3–5</sup> make them very attractive building blocks for drug delivery<sup>6</sup> and biochemical sensing. Special CNT/gelatin hybrid hydrogels were found to have the ability to separate proteins.<sup>7</sup> Furthermore, it was found that CNTs had actuator properties.<sup>8,9</sup> Thermoplastic elastomers filled with CNTs show remote actuator and good shape-recovery properties.<sup>10</sup>

One application field of CNTs is in soft matter, where CNT is not primarily used for its mechanical properties but for enhancing its capabilities, such as by modifying the electrical properties.<sup>11</sup>

Recently, hydrogels have also been used widely in a range of areas, including biological, medical, optical, structural, mechanical, material, and chemical engineering applications, because of their outstanding biological and physical features such as biocompatibility, transparency, impact resistance, water absorbance, and separation capability.<sup>12–14</sup> Considerable effort has been made to fabricate hydrogels with enhanced mechanical properties. Nevertheless, improving the mechanical properties is still a challenge, particularly when using pure hydrogels cross-linked with chemical, thermal, or irradiative stimuli.<sup>15,16</sup> Furthermore, it is important to control the mechanical properties of hydrogels in a more targeted and systematic manner in an effort to design a new hydrogel structure with optimized physical properties, which would be suitable not only for sustaining external forces from the environment but also for biological functionality, including cell adhesion and proliferation.<sup>17–20</sup> Equilibrium water content in hydrogels is one of their basic properties. A hydrogel with high water content is generally more advantageous for medical applications because

Received: July 3, 2012

Revised: November 19, 2012

of its permeability and biocompatibility.<sup>21</sup> Usually, a large swelling is accompanied by poor mechanical properties. There are several compromise alternatives between large swelling and good mechanical behavior. Increasing the cross-linking agent concentration can improve the mechanical properties but degrades the swelling. Copolymerization of hydrophilic monomer (which favors swelling) with a less hydrophilic monomer produces a hydrogel with good water absorbance and improved mechanical properties in the resulting hydrogel. Knowledge of swelling kinetics is important for designing controlled-released devices for drugs and agriculture pesticides based on swellable polymer matrices and for predicting the release rates of the active ingredients.<sup>22</sup> The swelling and shrinking behavior can be altered by the small change in environment like pH, temperature, electrical field, ionic strengths, and light.

Besides CNT, many other strategies were previously used to modify the properties of hydrogels. One method is the inclusion of ions in the hydrogel network, which leads to so-called ampholytic hydrogels that can augment the range of properties of hydrogels. There are two methods to prepare the ampholytic hydrogels: (1) copolymerizing an anionic monomer ( $\beta$ -carboxyethyl acrylate) with a cationic monomer<sup>23</sup> and (2) incorporating a zwitterionic monomer into the hydrogel network.<sup>24</sup>

Such polymers (e.g., polyacrylamide copolymer compounds) are useful for applications such as oil recovery,<sup>25</sup> drug delivery,<sup>26</sup> and as functional monomers used in the preparation of synthetic copolymers.<sup>27</sup> In these applications, both swelling behavior and mechanical properties are essential parameters.

When hydrogels are brought in contact with the water, it diffuses into the hydrogel and leads to swelling. Such swelling occurs due to the large-scale segmental motion, resulting in a bigger separation between hydrogel chains. Several publications evaluated the transport mechanism of water diffusion in the hydrogel matrix.<sup>28</sup> Results reported so far have concluded that the diffusion mechanism depends on several factors that include the hydrophilic and hydrophobic nature of the copolymers,<sup>29</sup> cross-linking density, and the effect of external stimuli such as a change in temperature and pH.<sup>30</sup> The complexity of the diffusion mechanisms makes it difficult to propose a universal model that accurately describes the diffusion mechanism and to calculate the diffusion coefficients. One of the classical models used to describe the diffusion process in this work is based on Fick's law:

$$\frac{dc}{dt} = D \frac{d^2c}{dx^2} \quad (1)$$

To enable reasonable modeling of the diffusion process, a complementary modeling method for early time approximation the power law approach (eq 2) is used.<sup>31,32</sup> The relative rate of diffusion ( $m_t/m_\infty$ ) is proportional ( $k$ ) to time raised to a power ( $n$ ). Whereas  $m_t$  and  $m_\infty$  denote the amount of solvent diffused into the gel at time  $t$  and at infinite time, respectively,  $k$  is a constant related to the structure of the network and  $n$  is a characteristic exponent of the transport mode of the solvent.<sup>33</sup>

$$\frac{m_t}{m_\infty} = kt^n \quad (2)$$

Depending on the relative rates of diffusion and polymer chains relaxation, three classes of diffusion mechanisms were observed:<sup>34</sup>

1. Case I (when  $n < 0.5$  Fickian): Fickian diffusion mechanism in which the rate of diffusion is much less than that of relaxation of the chains.
2. Case II (when  $n > 1$ ): diffusion, in which the diffusion is very rapid compared with the relaxation processes.
3. Case III (when  $0.5 < n < 1$  non-Fickian/anomalous): non-Fickian diffusion, which occurs when the diffusion and relaxation rates are comparable.

This paper reports the synthesis and characterization of thermoresponsive poly(*N*-isopropylacrylamide) (p-NIPAM)-*co*-zwitterionic hybrid hydrogels in filled with or without multiwalled carbon nanotubes (MWCNTs). The aim is to investigate the effect of supramolecular interaction among carboxylate CNTs and zwitterionic monomer concentration on the mechanical properties and diffusion mechanism in NIPAM-based hydrogels and to relate these to the chemical structure as the basis of the application of CNTs and zwitterionic monomers in the field of biomaterials, actuator, and artificial muscles. The swelling is conducted both in free state and in the rheometer under small oscillatory shear. We evaluate the structural changes during solvent diffusion in the rheometer, allowing for the online observation of the diffusion-induced changes in material behavior.

## EXPERIMENTAL SECTION

**Materials.** Methyl methacrylate (MMA, Merck), dibutyltin oxide (Merck), 3-(dimethylamino)-1-propanol, *N,N'*-methylenebis(acrylamide) (MBA, Sigma-Aldrich, 99%), *N,N,N',N'*-tetramethylethylenediamine (TMEDA, Fluka, >99%), ammonium peroxodisulfate (APS, Aldrich, >98%), 1,3-propane sultone (Aldrich, 98%), and 1,4-butane sultone (Aldrich, 98%) were used as received. NIPAM (Aldrich, 98%) was recrystallized from a 65:35 (v/v) mixture of hexane and benzene before use. Acetone was dried over CaCl<sub>2</sub> and distilled before use. All aqueous solutions were prepared with ultrapure water purified with a Milli-Q UV-Plus water purification system (Millipore, Bedford, MA). The water had a resistivity of  $>10^{18}$  M $\Omega$  cm<sup>-1</sup>. *N*-(3-(Dimethylamino)propyl)methacrylamide was synthesized by the transesterification of MMA and 3-(dimethylamino)-1-propanol in the presence of dibutyltin oxide as a catalyst, as previously reported.<sup>35</sup> Thin MWCNTs (purity >0.90), prepared by the chemical vapor deposition (CVD) process, were obtained from Nano Solution Co. Ltd. The MWCNTs had a diameter of 10 nm and a length of over 10  $\mu$ m.

**Synthesis.** *Synthesis of Zwitterionic Monomer N-(Methacryloylpropyl)-N,N-dimethyl-N-(3-sulfopropyl)ammonium Betaine (Zw).* A solution of 520 mg (50.4 mmol, 4.68 mL) of 1,4-butane sultone in 5 mL of acetone was added dropwise to a chilled stirred solution of 1.020 g (48 mmol) of *N*-(3-(dimethylamino)propyl)methacrylamide in 20 mL of dry acetone. The reaction mixture was stirred and increased to 40 °C, and the reaction was continued for 5 h. The white particles were formed gradually, and then the slurry was filtered and washed with a small amount of dry acetone. The filtrate was dried under dry nitrogen and kept in a refrigerator. The reaction yield was 78%.

Figure 1 demonstrates the <sup>1</sup>H NMR (400 MHz, D<sub>2</sub>O) results, which prove the purity of the obtained zwitterionic monomer: 5.986 s, 1 H, (H-C=); 5.59 s, 1 H, (H-C=); 4.12 t, 2 H, (O-CH<sub>2</sub>); 3.28 t, 2H, (N-CH<sub>2</sub>); 3.22 t, 2 H (N-CH<sub>2</sub>); 2.94 s, 6 H (N-CH<sub>3</sub>); 2.82 t, 2 H, (S-CH<sub>2</sub>); 2.07 m, 2 H (CH<sub>2</sub>); 1.78 s, 3 H (C-CH<sub>3</sub>), 1.65 m, 4 H (-CH<sub>2</sub>-).

**Preparation of Hydrogels. Purification and Carboxylation of Multiwalled Carbon Nanotubes (MWCNT).** 1 g of multiwalled CNTs (MWCNTs) was added gradually to 200 mL of concentrated nitric acid (69%, Daegeun grade) and stirred vigorously. The suspension was refluxed for 48 h at 120 °C in a 250 mL flask to remove the catalyst and side products of the carboxylation treatment. After cooling down to room temperature, the reaction mixture was poured into 500 mL of

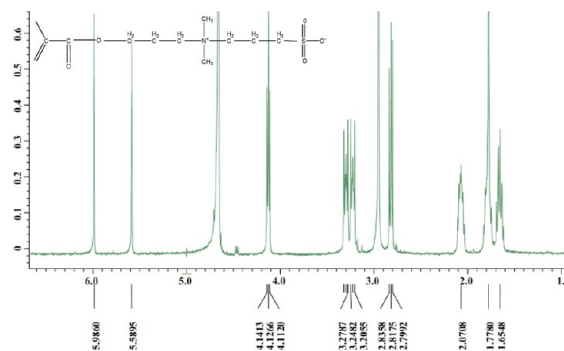


Figure 1.  $^1\text{H}$  NMR and chemical structure of Zw.

deionized water and then ultracentrifuged to separate the MWCNTs. Deionized water was added, and the centrifugation was repeated. This washing operation was repeated until the pH became the same as that of deionized water. The purified and functionalized MWCNT was dried in a vacuum oven at  $100\text{ }^\circ\text{C}$  overnight.

200 mg of the above MWCNTs was dispersed in 20 and 40 mL of deionized water to prepare 1 and 0.5 wt % MWCNTs suspensions, respectively. The mixture was initially sonicated for 60 min (Model WUC-A03H, Daihan Scientific Co. Ltd.), after which a stronger IKA sonicator (Power Sonic 50S, 350 W) was used for more intensive sonication treatment of the aqueous mixture (180 min). A microtip (1/4 in. in diameter) was immersed in the suspension, and the sonicator was run at 50% of maximum amplitude for  $3 \times 10$  min each at room temperature. Well-dispersed CNTs are known to have lower viscosities than those that have agglomerated.<sup>36</sup>

**Synthesis.** NIPAM, synthesized sulfobetaine zwitterionic (ZW) as monomers, and MBA as a cross-linker were added to a vial containing a solution of treated MWCNTs. The mixtures were stirred for 5 min, and the dissolved oxygen was removed by bubbling nitrogen through the solution for 1 h. An adequate amount of APS as initiator for free radical polymerization was added to the vial under nitrogen bubbling at room temperature.

After the solution was homogenized, TMEDA was added as an accelerator into the monomer solution to initiate the radical polymerization. After mild shaking for several seconds, the solution was transferred to the mold (PS, 43 mm inner diameter, 5 mm height). The polymerizations were continued for 6 h. After the polymerization, the prepared hydrogel was removed from the mold and immersed in double-distilled water at room temperature for at least 48 h, during which time the water was regularly refreshed in order to remove unreacted compounds.

The monomers and other reagent composition of the prepared hydrogels are listed in Table 1. The designation of the samples reflects the composition, where CNTx shows the amount of MWCNT in wt % of the total polymer content and Zwy stands for the molar concentration of zwitterionic monomer (in relation to the total monomer).

**Structural Characterization and Morphological Observation.** Variable pressure field emission scanning electron microscopy (FESEM; Zeiss Supra 40VP) was used to observe fractured morphologies of the as-prepared hydrogels. In order to evaluate the morphology and uniform dispersion of MWCNTs in the NIPAM hydrogels, dried hydrogels were fractured into fine particles and dispersed in ethanol and sonicated for 20 min.

Scanning electron microscopy (SEM; JEOL/JSM-6400) was used to observe the surface morphologies and fractured surfaces of the xerogels. Signals produced by secondary electrons, backscattered electrons, and characteristic X-rays resulting from interactions of the electron beam with atoms at or near the surface of the samples were amplified, and the morphologies of the images were obtained.

**Dynamic Swelling.** The compositional effect of MWCNT and zwitterions on the swelling behavior of the prepared hydrogels is the main objective of the present study. The gravimetric method was used to evaluate the swelling kinetics of the hydrogels. Dynamic swelling

Table 1. Hydrogels Composition<sup>a</sup>

sample	CNT [wt %]	molar fraction of zwitterionic monomer [mol %]	molar fraction of NIPAM [mol %]	amount of NIPAM [g]	cross-linker [g]
CNT0-Zw0			100	2	0.0675
CNT0.5-Zw0	0.5		100	2	0.0675
CNT1-Zw0	1		100	2	0.0675
CNT0.5-Zw10	0.5	10	90	1.8	0.0675
CNT0.5-Zw20	0.5	20	80	1.6	0.0675
CNT0-Zw10		10	90	0.9	0.034
CNT0-Zw20		20	80	0.8	0.034

<sup>a</sup>Solution concentrations of initiator and accelerator used are 1 g/mL water. A total of 50  $\mu\text{L}$  was added of both.

experiments were performed by placing the discs in distilled water at room temperature and measuring the amount of water absorbed. The weight of the samples increased over of time. The discs were removed from the water, gently wiped with a filter paper to remove any excess water, and then weighed. The discs mass, thickness, and diameter were measured at incremental time as the water was absorbed to monitor the dynamics of the hydrogel swelling.

The degree of swelling at different times can be calculated from the equation

$$W (\%) = (m_t - m_0/m_t) \times 100 \quad (3)$$

where  $m_t$  and  $m_0$  are the weights of the hydrogels at the predetermined time and at time 0 (xerogel), respectively.

**Rheological Measurements.** Dynamic-mechanical rheological measurements were performed on the swollen hydrogels until they reached equilibrium. The change in the mechanical properties of the hydrogels during swelling as a function of MWCNT and zwitterionic concentration was measured.

For dynamic rheological measurement, a parallel plate geometry with 20 mm diameter was used on a Malvern Kinexus rheometer in oscillatory mode. The hydrogels, with as little water as possible to obtain a gel flexible enough to fit in the aforementioned parallel plate geometry, were placed in a Petri dish  $60 \times 15$  mm fixed to the bottom plate (containing a Peltier heater). The upper plate geometry was pressed on to the gel with a constant normal force of 1 N ( $\rightarrow 3183$  Pa) to give a compressive deformation around 0.1. This normal force level was found to be sufficient to maintain a continuous adhesion of the sample to both plates throughout the test. The Petri dish was filled with distilled water, and the hydrogel was allowed to swell at  $25\text{ }^\circ\text{C}$ . Frequency sweep and time sweep experiments were used to analyze both elastic ( $G'$ ) and viscous ( $G''$ ) material response.

All experiments were carried out in the linear-viscoelastic regime using a stress  $\tau_0 = 50$  Pa, which leads to deformations  $\gamma_0 \approx 0.1\text{--}0.6\%$ , depending on the sample. The time-dependent data were measured at  $\omega = 0.16\text{ s}^{-1}$  (1 Hz). The frequency-dependent data were limited to an angular frequency  $\omega_{\text{max}}$  of  $60\text{ s}^{-1}$  due to the low modulus and low phase angle, which lead to geometry inertia artifacts.

This setup, while being able to monitor the change of properties as a function of water uptake, suffers potentially from three experimental artifacts.

First, the sample is significantly larger than the 20 mm plate, hence leading to a slightly higher modulus than found in reality. This can be compensated for by comparing the data with elongational data and shear data with a defined sample shape and swelling state. The correction is around 50%, which is in the range expected and can be translated as a geometry that is apparently larger by 10%. Considering that the sample is swelling in all three dimensions during the test, this

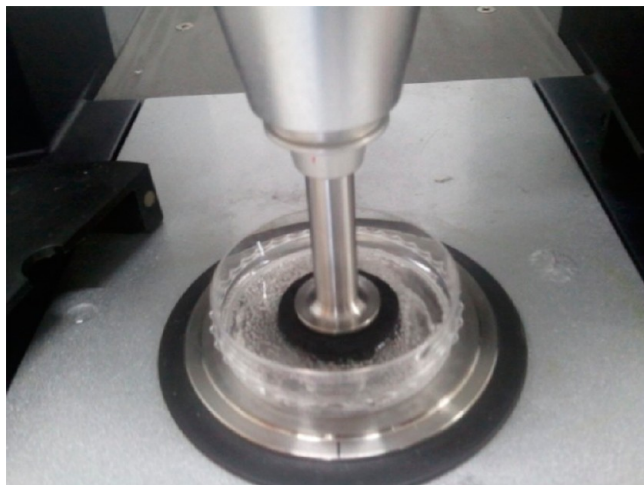


Figure 2. Experimental setup of the swelling.

artifact is unavoidable and needs to be corrected for. Fortunately, using a sample that is significantly too large in diameter for the geometry enables the problem to be simplified, as this leads to a constant correction factor because the apparent increase in geometry diameter is limited to a value of approximately the height. Hence, using a sample that is significantly larger than the diameter +  $2 \times$  gap will lead to an approximately constant error, which can be easily compensated for.

Second, the compressive stress on the sample, albeit relatively small, will somewhat influence the swelling kinetics, which can be extrapolated by comparing the swelling rates for different compressive stresses. Third, the surface of the sample is reduced due to the two 20 mm contact points. Furthermore, an additional unknown fraction of the lower side of the sample is stuck to the lower plate and, therefore, needs a longer diffusion path than the sample floating freely in the water—as performed in the normal swelling tests. The last two artifacts lead to slower swelling kinetics.

These artifacts have been discussed elsewhere.<sup>37</sup> As the phase angle  $\delta$  is not influenced by the artifacts significantly, and the changes in the

material behavior are shown best by  $\delta$ ; this quantity is discussed primarily in this article.

**Elongational Rheology.** Samples for elongational rheology were cut from the prepared sample disks using wetted razor blades. The thickness of the sample disks was around 4 mm. Slices of approximately 1.5–2.5 mm width were cut from the samples having a length of 25–30 mm.

Elongational measurements were performed with a TA Instruments ARES using an EVF (elongational viscosity fixture) geometry. Unlike in the standard operation, the samples were not clamped on the sample drums but superglued, which ensured proper adhesion and avoided high notch stresses, which can easily lead to sample rupture during sample loading and early stages of the experiment. The experiments were conducted under constant Hencky strain rate  $\dot{\epsilon}$ ,<sup>38</sup> which allows for a physically more reasonable determination of elongation at break  $\epsilon_H^{\max}$  and stress at break  $\sigma_H^{\max}$  than classical Cauchy terms.<sup>39</sup>

Hencky strain rates of  $\dot{\epsilon} = 10, 1, 0.1,$  and  $0.01 \text{ s}^{-1}$  were conducted to obtain information on the gel-like structure of the material, which theoretically should be time- and, thus, strain-rate-independent. Furthermore, the different strain rates also allow for a determination of the modulus of the gel from the linear part of the time-dependent elongational viscosity  $\eta_e(t, \dot{\epsilon})$ , which is found for a Hencky strain  $\epsilon_H < 0.2$ – $0.5$ , depending on the structure of the material. The test setup has been described elsewhere in full detail.<sup>40–43</sup>

## RESULTS

**Electron Microscopy.** Figure 3 shows the FESEM images of the hydrogels containing significant amounts of solvent. The CNT0-Zw10 sample (Figure 3c) clearly shows an entirely different structure from CNT0.5-Zw10 (Figure 3a). As clusters of CNTs were not observed in any of the samples, it is concluded that the MWCNTs are uniformly dispersed into the hydrogels. The CNT0.5-Zw10 sample (Figure 3a) is clearly seen to be CNT-coated with NIPAM layers, as the thickness of the fibrous structures is 16 nm vs the 10 nm of the MWCNTs used for the material.

It is concluded that the carboxyl and hydroxyl groups created at the surface of MWCNTs during acid treatment stabilize the

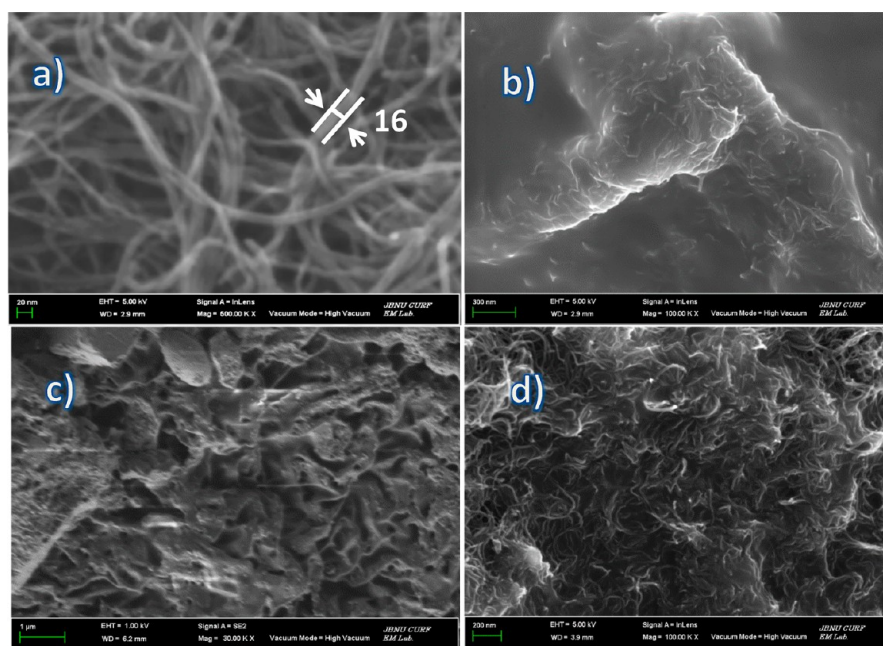
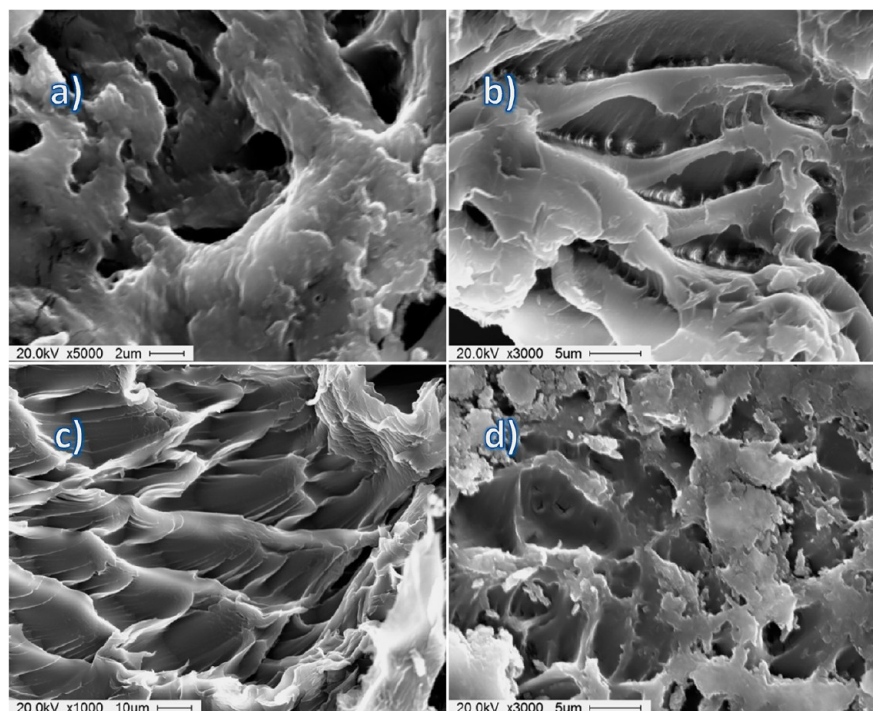


Figure 3. FESEM images of (a) CNT0.5-Zw10, scale bar 20 nm; (b) CNT0.5-Zw20, scale bar 300 nm; (c) CNT0-Zw10, scale bar 1000 nm = 1  $\mu\text{m}$ ; and (d) CNT1-Zw0, scale bar 200 nm.



**Figure 4.** SEM images of (a) CNT0-Zw0, scale bar 2  $\mu\text{m}$ ; (b) CNT0.5-Zw20, scale bar 5  $\mu\text{m}$ ; (c) CNT0-Zw10, scale bar 10  $\mu\text{m}$ ; and (d) CNT0-Zw0, scale bar 5  $\mu\text{m}$ .

MWCNT dispersions due to their strong interaction with the zwitterion-containing matrix. As CNT1-Zw0 (Figure 3d) does not show this increase in thickness of the CNTs, it is concluded that this sample does not contain CNTs coated with the pure pNIPAM matrix. This is a strong indicator that the interaction with the functional groups, probably with the  $-\text{NH}_2$  of the zwitterions, is responsible for the encapsulation of the CNTs.<sup>44</sup> Figure 3b shows large fibrous structures with a thickness of several hundred micrometers in CNT0.5-Zw20, which seem to be made up of weakly bundled CNTs complexed by the zwitterions, presumably leading to the significantly different properties of the hydrogels containing CNT and zwitterions compared to the previously characterized pNIPAM hydrogels.

Figure 4 shows SEM images of dried hydrogels (xerogels) predominantly without CNT, which cannot be characterized by FESEM as well as the CNT-containing hydrogels, due to the local heat produced by the electron beam. When comparing the samples containing zwitterions (Figure 4b,c) to the pure pNIPAM-hydrogel (Figure 4a,d), it is clear that zwitterions cause a flatter surface structure on a small range and leaf, arc, or flat on a length scale of  $\sim 100 \mu\text{m}$ . This can be attributed to the high interaction between the zwitterionic moieties, which, especially at low water contents, hold the hydrogel together strongly and, thus, prevent ductile-like cracks, leading to flat breaking surfaces, which, in turn, due to the elasticity of the samples (cf. Figure 12) can form some daughter cracks, leading to the arcs and lamellae described.

CNTs (Figure 4b) lead to finer fracture surface structures, as the encapsulated CNTs lead to local zwitterion and, consequently, polymer density fluctuations, which open up paths for the cracks to penetrate into the sample. Furthermore, the sharp ends of CNTs having an end radius of about 5 nm are very strong stress raisers, which can induce the fracture in the polymer-depleted vicinity of the CNT ends. At the same time, the CNTs have the ability to bridge cracks, as evidenced in the

structures at the bottom of the deepest pits, which are sized as would be expected for polymer-covered CNTs. Hence, the cracks in xerogels containing CNT can be stopped by CNTs bridging the crack tips.

**Investigation of Water Diffusion in Hydrogel.** The swelling properties were evaluated by free swelling experiments, which were evaluated using eq 2. The exponents  $n$  obtained are listed in Table 2. The maximum degree of swelling normalized by the polymer weight  $m_\infty/m_0$  shows that the addition of Zw or CNT increases the maximum water uptake.

**Table 2.** Summary of Diffusion Data

sample	characteristic exponent $n$	diffusion mechanism	$m_\infty/m_0$	$m_\infty/m$ (solid)
CNT0-Zw0	0.33	Fickian	4.4	10.36
CNT0.5-Zw0	0.42	Fickian	5.7	11.22
CNT1-Zw0	0.45	Fickian	7.2	10.74
CNT0.5-Zw10	0.47	Fickian	5.9	11.58
CNT0.5-Zw20	0.45	Fickian	8.3	12.8
CNT0-Zw10	0.66 ( $t \leq 140 \text{ min}$ ) 0.35 ( $t \geq 140 \text{ min}$ )	non-Fickian Fickian	7.9	10.5
CNT0-Zw20	0.66 ( $t \leq 140 \text{ min}$ ) 0.38 ( $t \geq 140 \text{ min}$ )	non-Fickian Fickian	8.2	13.8

Figure 5 shows the swelling data of the different hydrogels, which were evaluated by eq 2, with the first and last data points omitted. For most samples, however, the first data point roughly lies on the extrapolated regression line, indicating that the diffusion mechanism is already close to its equilibrium at low times (30 min).

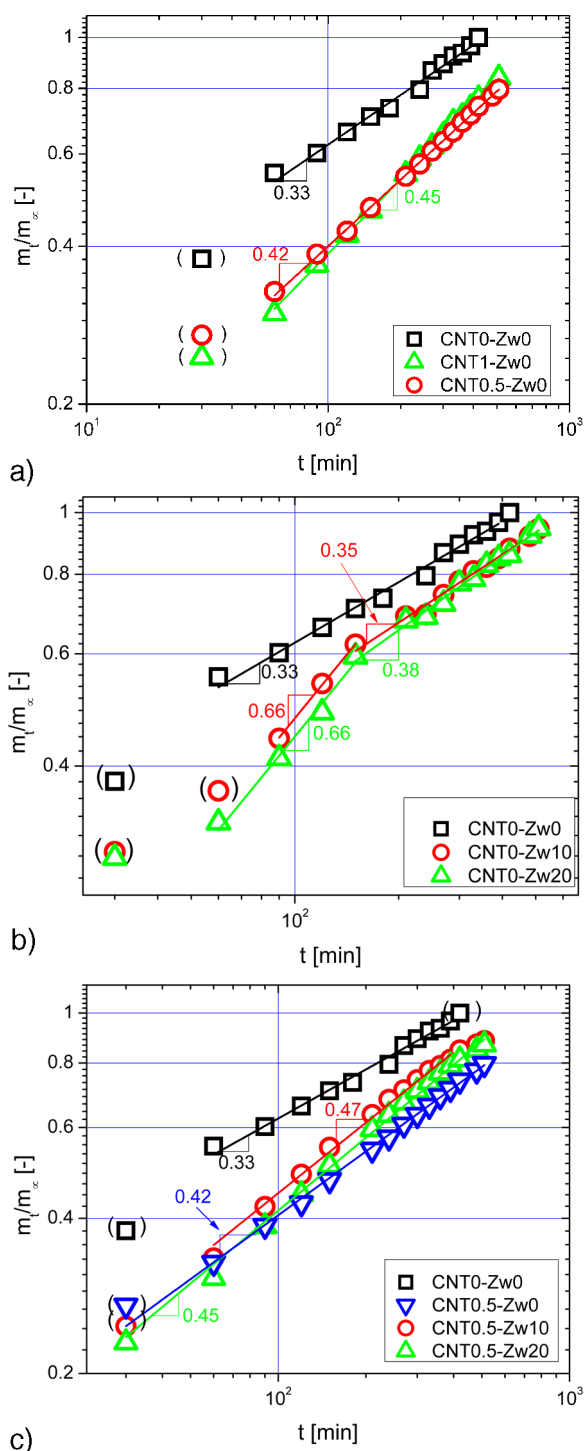


**Figure 5.** Swelling as a function of time: (a) hydrogels with CNT, (b) hydrogels with Zw, and (c) hydrogels with CNT and Zw.

The pure pNIPAM hydrogel (CNT0-Zw0, Figure 5a) shows a diffusion coefficient  $n$  of 0.33, meaning that the diffusion is significantly slower than the chain relaxation, which is further clarified by the rheological data that are presented below. Adding CNT increases the slope  $n$  to 0.42 and 0.45 for 0.5% and 1% CNT, respectively, indicating that the relaxation is slower than the diffusion. Furthermore, the diffusion is slowed down in terms of  $m_t/m_\infty(t)$ , as the values lie lower than for CNT0-Zw0.

When considering the gels containing zwitterions (Figure 5b), the diffusion changes its characteristic around  $m_t/m_\infty = 0.6$  for both Zw samples (CNT0-Zw10 and CNT0-Zw20). At lower swelling ratios/lower times ( $t \leq 140$  min), the slope  $n \approx 0.66$ , indicating an anomalous diffusion, while for higher swelling ratios/longer times, the exponent is almost the same as that for CNT0-Zw0 ( $n = 0.35/0.38$ ), indicating the action of normal Fickian swelling in this regime. Furthermore, the significantly slower slope that is apparent at short times ( $t \leq 50$  min) must, however, include the omitted data points and, thus, the startup effects. Hence, this cannot be quantified. Explaining this change in swelling behavior necessitates a discussion of the rheological properties, which is presented in the Conclusions section.

Figure 5c shows the effect of the CNT and Zw addition to the hydrogel. The behaviors of CNT0.5-Zw10 and CNT0.5-Zw20 are very similar to that of CNT0.5-Zw0, whose slope is slightly lower. Unlike the sample containing only Zw and no CNT, the illustrated behavior does not show two clear regimes. Nevertheless, a small change of slope remains present for these materials. Hence, the effect of the zwitterions on the diffusion behavior is almost negligible in the presence of CNT.

To elucidate the processes happening in the hydrogels containing zwitterions, the water content in relation to the solids content should be investigated, for which the solids content  $m_0 = 0.6$  g (0.603 and 0.606 g for the CNT-containing samples) is used to normalize the weight of the sample  $m$  at time  $t$ . Figure 6 shows the data for the samples containing

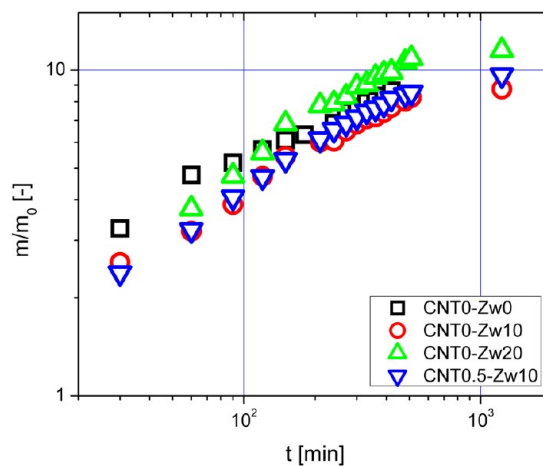


**Figure 6.** Ratio of total weight to solids weight as a function of time.

zwitterions only (CNT0-Zw10 and CNT0-Zw20) and for CNT0-Zw0 and CNT0.5-Zw10. Beyond the superficially similar curves, closer inspection reveals that CNT0-Zw10 and CNT0-Zw20 are significantly below CNT0-Zw0 for  $t < 100$  min. At 150 min, the slope of CNT0-Zw10 and CNT0-Zw20 changes, which is at the same time as the mass of the Zw-containing samples reaches the curve of CNT0-Zw0; i.e., the swelling of CNT0-Zw10 and CNT0-Zw20 is significantly slower in the beginning and then speeds up and slows down at the point where it meets the water uptake of CNT0-Zw0.

These results provide an explanation for the behavior. Initially, the hydrogel's zwitterions in the chains are only separated by very little water, which allows for strong zwitterionic interactions, as the hydrostatic forces are too weak to temporarily separate them. As a consequence, the

swelling is hindered because the zwitterions' interactions are strong and thus do not make space for the water to diffuse in.<sup>45</sup> This leads to a less swelling at short times, which, however, cannot be quantified due to the aforementioned startup effects. At a critical water concentration, the interactions between the zwitterions become so weak that they no longer hinder the water uptake. At this time, the osmotic pressure to dilute the (zwitter)ions sets in, which significantly increases the swelling rate. Furthermore, the loose interactions between the zwitterions slow down the relaxation of the increasingly free chain segments, which increases the diffusion exponent  $n$ . This fast diffusion is slowed down when the swelling degree of CNT0-Zw0 is reached, which is caused by the twin facts that the diffusion rate is now limited by the NIPAM-network and that the zwitterions are so greatly diluted that they no longer have a significant osmotic contribution.

**Shear Rheology.** Figure 7 shows the rheological data as a function of swelling time. In comparison to the free swelling

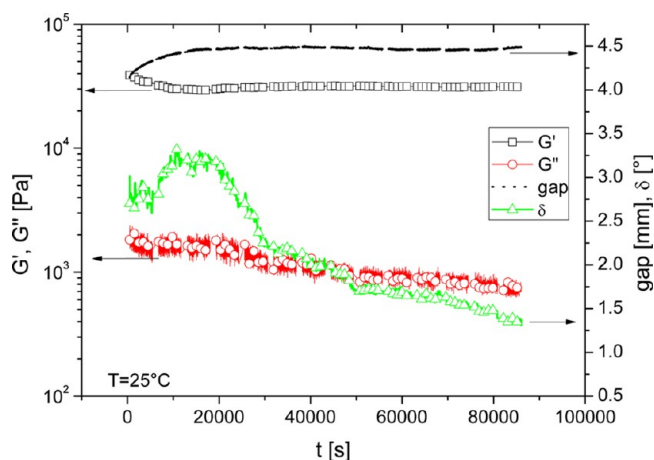


**Figure 7.** Storage modulus  $G'$ , loss modulus  $G''$ , phase angle  $\delta$ , and gap as a function of swelling time for sample CNT1-Zw0.

experiments, the samples were loaded with significantly more water, as the less swollen samples were too stiff for loading them. While the storage modulus  $G'$  only decreases slightly at longer times, due to the softening of the sample, the gap continues increasing, suggesting that the swelling is not yet in equilibrium. Loss modulus  $G''$  and phase angle  $\delta$  continue decreasing for almost 20 h until reaching steady state.

The reduction of the damping of the sample, i.e., the decrease of  $\delta$ , is due to the stretching of the chains by the water diffusing in. As the chain segments between two cross-links are stretched further, less energy can be dissipated by the dangling of the segments. At equilibrium swelling, consequently,  $\delta$  is very low, indicating that only very little dissipation is possible. This also suggests that very few free chain ends or free chains are present in the sample. The latter point is also important for applications, as the absence of free chains prevents the washing out of any polymeric component of the hydrogel, thus making it safer for medical applications.

The time-resolved plots of  $G'(\omega)$  and  $G''(\omega)$  are shown in Figure 8. For the different samples,  $G'(\omega)$  shows a more or less constant value, while  $G''(\omega)$  is lower by a factor 10–1000. The swelling time is color coded starting from red and going to blue. Figure 8a shows CNT0-Zw0, the standard PNIPAM-hydrogel, whose properties show almost no change as a function of time and  $G''(\omega)$  is very low, while CNT0-Zw20 (Figure 8b) shows a

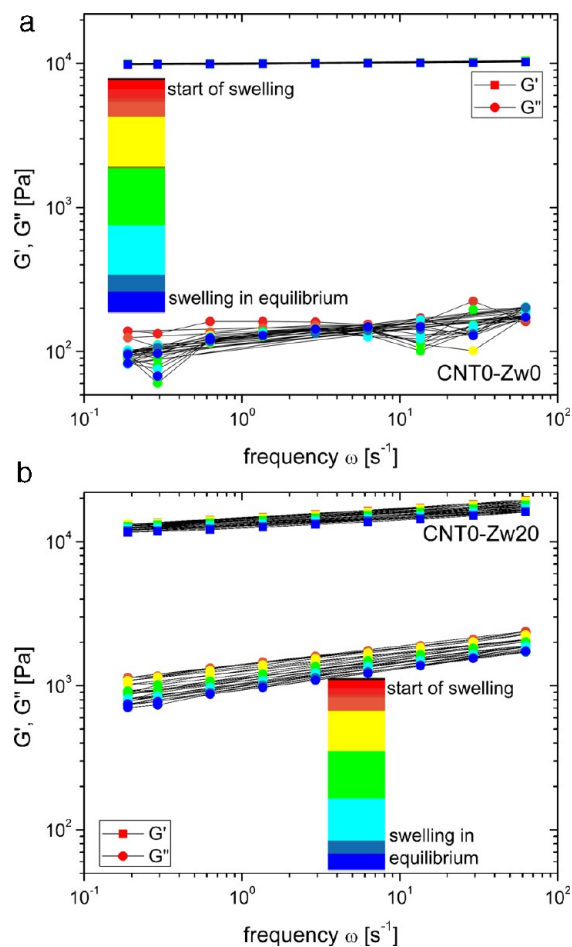


**Figure 8.** Time-resolved  $G'(\omega)$  and  $G''(\omega)$  of (a) CNT0-Zw0 and (b) CNT0-Zw20.

significantly higher  $G''(\omega)$  and a significant change with time. Also, CNT0-Zw20 shows a significant decrease of  $G'(\omega)$ , while  $G'(\omega)$  of CNT0-Zw0 is almost constant. The other plots are given in the Supporting Information, as in the following  $\delta(\omega)$  will be discussed, as this quantity shows the changes in a way easier to comprehend.

In Figure 9, the frequency phase angle  $\delta(\omega)$  is discussed at different times of water uptake at 25 °C. The filled symbols (low) were taken in the beginning of the swelling, when the swelling ratio was around 3. The open symbols were taken at the end of the swelling with equilibrium water content (high). In general,  $\delta(\omega)$  decreases with increasing swelling due to the increasing stretch of the chain segments that results from the increased water incorporation (cf. Figure 7). However, that the change between “low” and “high” is lowest for the pure pNIPAM hydrogels (CNT0-Zw0), followed by the Zw hydrogels (CNT0-Zw10 and CNT0-Zw20). Pure pNIPAM hydrogels (CNT0-Zw0) have an almost frequency-independent phase angle  $\delta(\omega)$  of  $\approx 0.8^\circ$ , which means that almost no energy dissipation is found in the frequency range. This indicates the absence of any relaxation processes within the frequency range of the experiment. As the samples are true covalent hydrogels, it can be concluded that no further relaxation occurs at lower frequencies, which was also confirmed by the finding that the sample shape does not change under gravity after initial sagging. As the relaxation process typically is detectable in terms of  $\delta(\omega)$  at least 2 orders of magnitude away from the

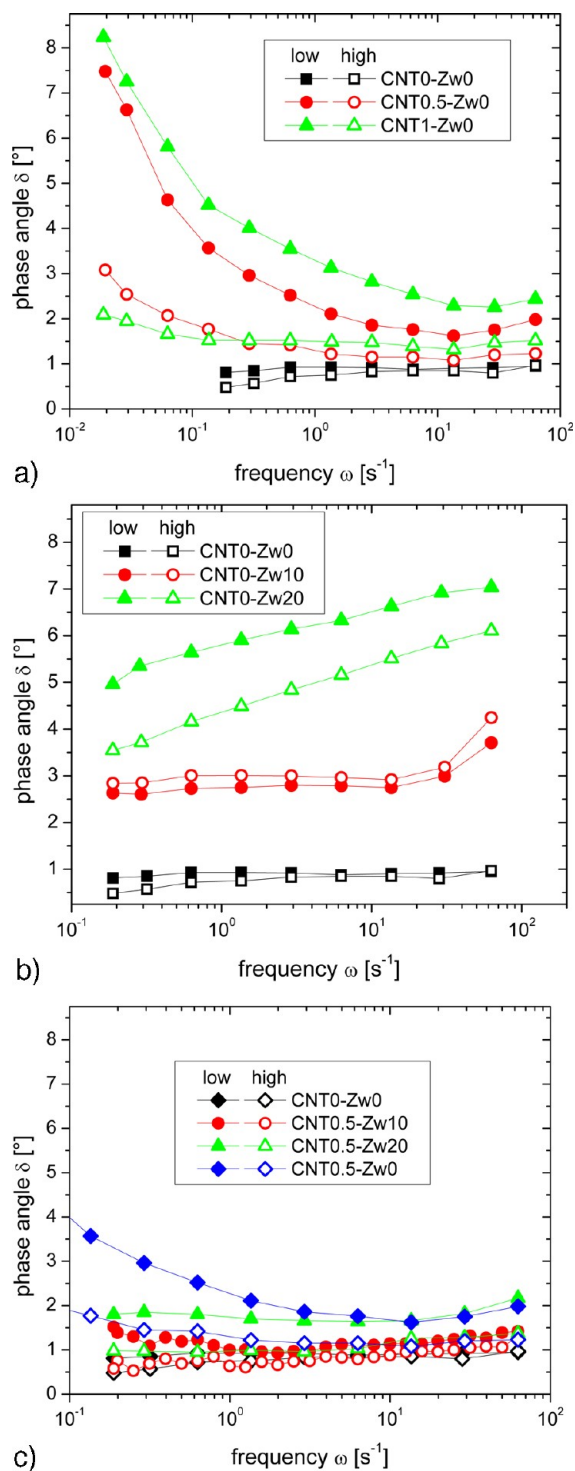


**Figure 9.** Phase angle  $\delta(\omega)$  as a function of frequency at different swelling times: (a) hydrogels with CNT, (b) hydrogels with Zw, and (c) hydrogels with CNT and Zw. Temperature  $T = 25\text{ }^{\circ}\text{C}$ .

relaxation time, at which it occurs,<sup>43,46</sup> the fast relaxation times have to be in the sub-millisecond range.

This offers an interesting insight into the molecular structure of the CNT0-Zw0 hydrogel. When considering the structure of this hydrogel and the changes occurring during the swelling, it is clear that free chain ends as well as long nonstretched segments between two cross-linking points are candidates for energy dissipation. From the reaction mechanism and the prior

deswelling, we conclude that both species must exist. The dangling chain ends exist at a constant concentration independent of the swelling state, but the stretching of the network segments depends on the amount of water absorbed. The difference in behavior for the CNT0-Zw0 hydrogel is very small at low and high water content, indicating that the unstretched network segments must only have a minor effect on the behavior, as otherwise the observed change of energy dissipation would be greater. Hence, the dangling chain ends account for most of the observed damping  $\delta(\omega)$ . This is confirmation of the time-dependent data (Figure 7).

Figure 9a shows that the addition of CNT leads to a high phase angle at low frequencies, which means that some slow processes can occur. This is in agreement with the higher exponent  $n$  of the swelling for these systems, which indicates that the swelling—a very slow process at very low frequency—occurs on roughly the same time scale as the relaxation. Hence, it is logical that the swelling is delayed in comparison to the pure pNIPAM hydrogel (CNT0-Zw0, Figures 5 and 6) and that the exponent is close to anomalous diffusion. Considering the composition of these samples, it is clear that the dissipation originates from the interaction of the pNIPAM chains with the CNT. With further water penetration, this energy dissipating process becomes weaker and slower due to the depletion and dilution of the CNTs and the surrounding pNIPAM chains.

The zwitterionic samples show a much higher damping at high frequencies (Figure 9b) due to the interaction of the zwitterions with each other. This interaction weakens with increasing water content, as the concentration of zwitterions decreases proportional to the water content. However, when assuming that  $\delta$  should be proportional to the Zw concentration, approximately the right difference is found between CNT0-Zw0, CNT0-Zw10, and CNT0-Zw20 ( $\approx 3^{\circ}$  per 10% Zw), but the swelling dependence is much weaker than that expected from a simple dilution, which is  $\delta \approx 1.5^{\circ}$  (at 1 Hz) for swollen CNT0-Zw20 and not  $4.5^{\circ}$ . CNT0-Zw10 exhibits almost no swelling dependence.

Hence, it is concluded that the swelling does not separate the zwitterionic groups so much that they can no longer interact. Instead, they form local temporary concentration fluctuations, which move with the Brownian motions of the chains. The reduction of  $\delta(\omega)$  is then due to a weakening of these local clusters of interaction. These conclusions agree with the findings of Lee and Chen<sup>47</sup> and Lowe et al.<sup>45</sup>

The hydrogels containing CNT and zwitterions show yet another behavior (Figure 9c). CNT leads to higher  $\delta$  at low  $\omega$  and Zw to a higher  $\delta$  at high  $\omega$ . CNT0.5-Zw10 shows a constant low  $\delta(\omega)$ , which is almost identical to CNT0-Zw0 in the swollen state. A small upturn at low  $\omega$  is found only in the “low” swollen state, which indicates that a weaker version of the processes, observed for CNT0.5-Zw0, also occurs here. The CNT0.5-Zw20 sample shows a weaker version of the behavior of CNT0-Zw10 in the “low” swelling state and basically the same behavior as CNT0-Zw0 in the “high” swollen state.

On the basis of these findings and the swelling data, it can be concluded that CNT adsorbs zwitterions on its surface, which has two consequences. First, the anomalous swelling induced by zwitterions without CNT cannot occur, as the zwitterions cannot initially hinder diffusion. This lowers  $\delta(\omega)$  to  $1^{\circ}$ – $2^{\circ}$ . Interestingly, CNT0.5-Zw10 and CNT0.5-Zw20 differ distinctly in their “low” swelling state behavior, which can be attributed to the balance between CNT and zwitterion concentration. 10% Zw is insufficient to prevent the relaxation

process of CNT completely, leading to the small upturn at low  $\omega$ . 20% Zw cannot be absorbed on the CNT completely, leaving some zwitterions unabsorbed and, thus, increasing  $\delta(\omega)$  by about  $1^\circ$ . These results explicitly show that the swelling behavior of these gels is affected by the internal structure and the content of the zwitterions in the polymeric gels.

**Elongational Rheology.** Figure 10 shows the elongational data of the hydrogel CNT0.5-Zw0, which is representative of

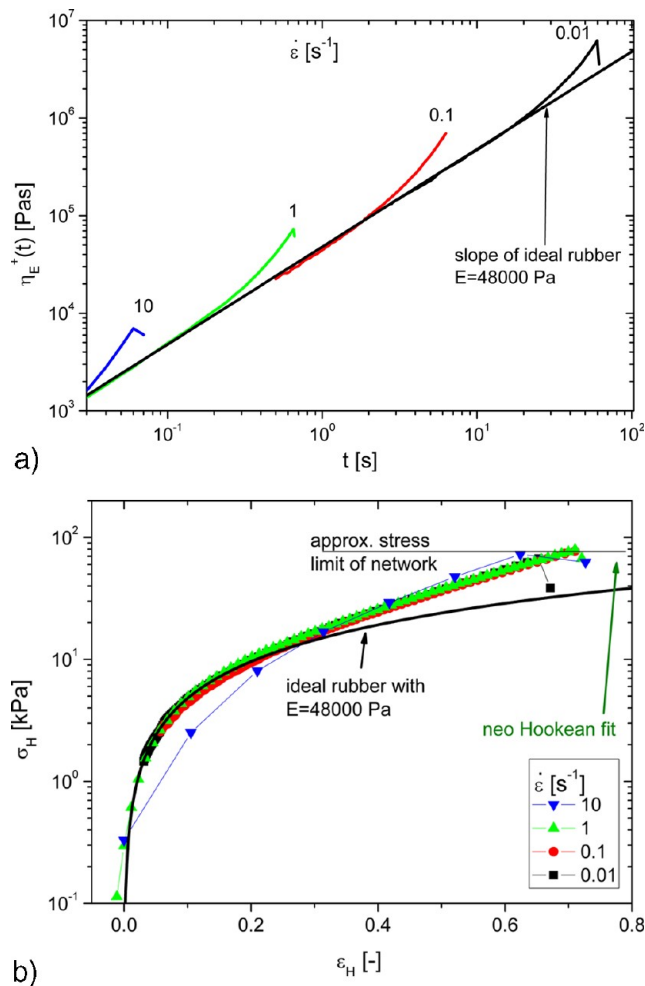


**Figure 10.** Elongational rheological data of the hydrogel CNT0.5-Zw0 with 0.5% CNT: (a) time-dependent elongational viscosity  $\eta_e(t, \dot{\epsilon})$  and (b) Hencky stress as a function of Hencky strain.

the other hydrogels. Figure 10a demonstrates that for  $\epsilon_H < 0.25$  the elongational viscosity  $\eta_e(t, \dot{\epsilon})$  increases with a slope of 1 in log–log scaling, which is typical for ideal rubbers and can be fitted with

$$E_0 = \eta_e(t, \dot{\epsilon})/t \quad (4)$$

which in this case yields  $E_0 = 48\,000$  Pa, a relatively high value for a hydrogel.

For larger Hencky strains  $\epsilon_H$ , the viscosity exceeds this threshold, as the elongational deformation leads to a structural orientation that stiffens the network. The strain hardening found is related to the structure of the molecules.<sup>42</sup> One might argue that this strain hardening is caused by the 3D-tensorial behavior, which can be modeled by a neo-Hookean model:<sup>48</sup>

$$\sigma_E = G(\lambda^2 + 1/\lambda) \quad \text{with } \epsilon_H = \ln \lambda \quad (5)$$

where  $G$  is the shear modulus, i.e.,  $G = 3 \times E_0$ . Figure 10b shows the stress as a function of strain  $\sigma_H(\epsilon_H)$ . While the data for  $\dot{\epsilon} = 10 \text{ s}^{-1}$  slightly deviates, the lower elongational rates roughly agree. The disagreement of  $\dot{\epsilon} = 10 \text{ s}^{-1}$  is due to the high speed of the experiment, which lasts only 0.055 s until rupture and which indicates that the inertias in the torque transducer and the sample itself play a role. Nevertheless, the similarity of the shape and measured values indicates that these data can be considered valid as well. The prediction of  $\sigma_H(\epsilon_H)$  assuming a constant modulus  $E_0$  is given in Figure 10b as the thick line, which describes the data well up to  $\epsilon_H \approx 0.25$ . Following this, a power law increase is found due to the strain hardening of the system. At  $\sigma_H^{\max} \approx 78$  kPa, the tensile strength of the network is reached, which is a relatively high value for a NIPAM-based hydrogel. Some hydrogels with significantly lower stiffness, higher elongation at break  $\epsilon_H^{\max}$ , and ionic tensile surfmer micelles show a higher  $\sigma_H^{\max}$ .<sup>42</sup> When comparing the data with the predictions from neo-Hookean model (eq 5), it becomes obvious from Figure 10b that the neo-Hookean model (eq 5) predicts a higher stress at high  $\epsilon_H$  than the classical Hookean model but that the experimentally found stresses are still higher than neo-Hookean model. Hence, it is concluded that while part of the strain-hardening can be explained by the 3D-stress tensor, the material is still strain hardening.

Figure 11 compares the hydrogels containing different amounts of CNT. The modulus is given as the average of the

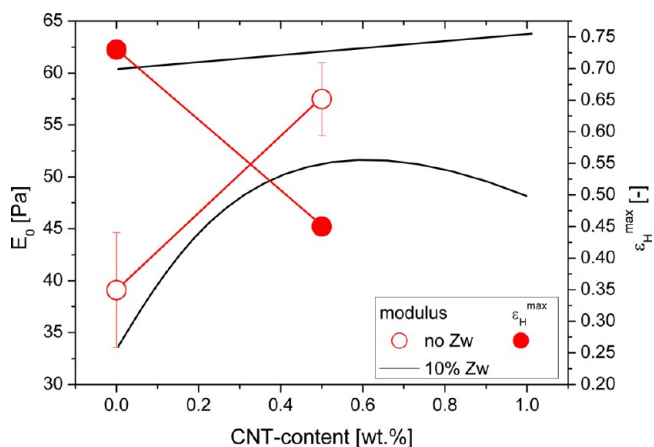


**Figure 11.** Modulus and maximum elongation  $\epsilon_H^{\max}$  as a function of CNT content. Lines are added to guide the eye.

value in elongation  $E_0$  and the triple value of the corrected shear modulus  $G_0$  in the swelling test, which assuming incompressible fluids and simple elongation should be identical.<sup>49</sup>

An increase of CNT content affords a small but clear increase in strain at break  $\epsilon_H^{\max}$ , which is not obeyed by the samples with zwitterions (red dots). The modulus goes through a maximum around 0.5 wt % CNT. At 1 wt % CNT, the stiffness of the hydrogel is significantly lower, which can only mean that the network is weaker than for the sample with 0.5% CNT. This behavior can probably be attributed to the adsorption of some NIPAM on the surface of the CNTs (cf. Figure 3a), which depletes the network and thus lowers the stiffness of the hydrogel. The increased stretchability of these materials underlines these findings and indicates that the network is also depleted to some degree for CNT0.5-Zw0, but less than

that for the CNT1-Zw0 hydrogel. Hence, CNT0.5-Zw0 has a higher modulus. This behavior is similar to the adsorption of NIPAM in surfmer micelles reported earlier.<sup>42</sup>

When comparing the samples with and without zwitterions (Figure 12), the functional group adds about 8 kPa in terms of

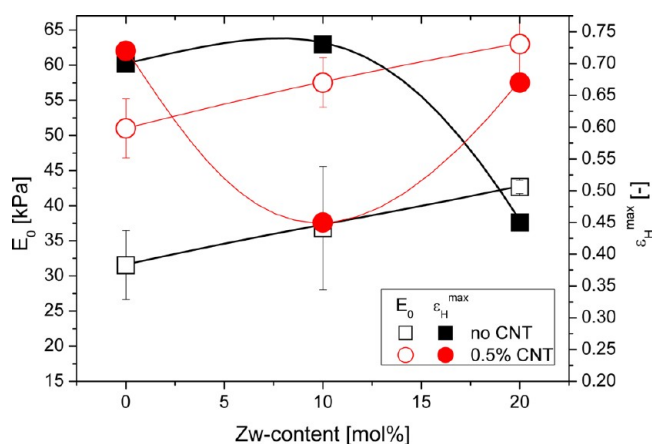


**Figure 12.** Modulus and maximum elongation  $\epsilon_H^{\max}$  as a function of Zw content. Lines are added to guide the eye.

stiffness for 0 and 10 wt % Zw, which is equal to a decrease of the cross-linking molar mass from 17 000 to 14 000 g/mol and which indicates that 10 wt % Zw is as effective as 0.44 wt % cross-linker. However, both stiffness and elongation at break are significantly decreased for 20 wt % Zw, probably due to the zwitterions slightly disturbing the formation of cross-links during polymerization and, thus, giving a lower modulus than expected. The lower  $\epsilon_H^{\max}$  can be understood as a consequence of the zwitterions creating clusters of interaction, which then induce local stress risers that make the sample fail prematurely. Interestingly, adding CNT leads to a minimum in  $\epsilon_H^{\max}$  followed by this quantity returning to approximately its original value. This can be understood as the consequence of the fact that Zw encapsulate CNTs. It is shown in Figure 9 that a little more than 10% Zw fully encapsulate the CNTs, which means that the sample CNT0.5-Zw20 has some free Zw, which, just like for CNT0-Zw10, leads to a stabilization of cracks due to zwitterionic interactions before leading to too big “holes” in the network (CNT0-Zw20).

## CONCLUSIONS

The results show some significant differences between hydrogels containing only NIPAM, NIPAM and CNT, and NIPAM and Zw and CNT on one hand and NIPAM and Zw on the other. The swelling properties suggest a Fickian behavior for the first group and a non-Fickian behavior for the second group, which is highly anomalous, as it is divided into three different stages. Figure 13 shows this behavior schematically.

A non-Fickian behavior indicates that the chain relaxation and diffusion are comparable. When looking at the NIPAM and Zw hydrogels in terms of their rheological properties, it is obvious that their frequency-dependent phase angle  $\delta(\omega)$  is significantly higher ( $3^\circ$ – $7^\circ$  in the range between  $\omega = 60$  and  $0.1 \text{ s}^{-1}$ ) than for the other hydrogels ( $0.5^\circ$ – $2^\circ$ ). At the same time  $G'(\omega)$  decreases significantly for decreasing frequency, which is logical considering the connection between  $\delta(\omega)$  and  $d \log |G^*|/d \log \omega$ , as can be derived from the Kramers–Kronig relations.<sup>50</sup> This is clearly associated with the presence of a

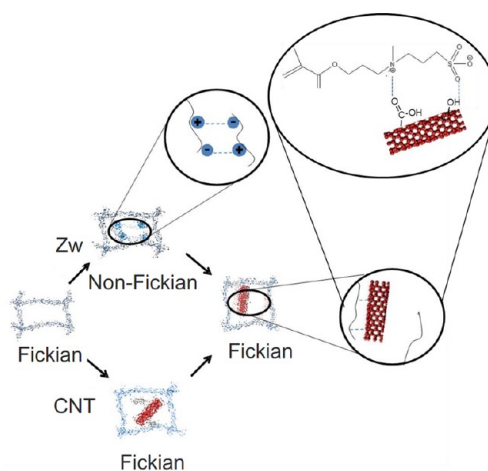


**Figure 13.** Schematic of the structure and diffusion mechanism.

relaxation mode at slightly higher frequencies than measured. Additionally, this relaxation mode persists from almost unswollen to equilibrium swollen state, suggesting an interaction that does not depend significantly on the water content. The most logical explanation is the interaction of the zwitterionic groups with each other, significantly slowing down the relaxation of the dangling or random chain segment.

In the elongational tests, this can be observed as a significantly higher modulus for 10% Zw, which, however, reverses for the CNT0-Zw20 sample. Further, the CNT0-Zw20 sample is very brittle, which shows in  $\epsilon_H^{\max} \approx 0.45$ , a rather low value for a hydrogel. This suggests that the zwitterions disturb the cross-linking-reaction, leading to a gel with a significant amount of errors in the cross-linked network and, hence, a brittle sample.

The swelling behavior of the Zw-containing hydrogels shows a clear change of slope from non-Fickian ( $n \approx 0.65$ ) to Fickian for swelling times longer than 140 min. This can be explained by the increasing dilution of the zwitterions, the content of which is reduced from 10% or 20% of the sample mass in the beginning to less than 1% in equilibrium swelling state. Hence, the zwitterions stick together so strongly at low swelling state that they slow down the dilution by water, which leads to a low slope in the swelling curve (Figure 5). Once a certain threshold in the water content is exceeded, the swelling speeds up significantly as the half-diluted zwitterions “want to be diluted”. Once the water content reaches that of the pure pNIPAM gel (CNT0-Zw0), the water uptake rate of the pNIPAM network dominates, leading to a slower uptake rate that is closely correlated to a normal pNIPAM hydrogel.

In terms of rheology, the second regime has a high phase angle  $\delta$  at high  $\omega$ , which is lower at equilibrium swelling. The increasing dilution of the zwitterions introduces two effects. First, fewer zwitterions are present in the sample measured (a round section of the sample with a diameter of around 22 mm) than at a lower swelling state. Second, the higher swelling state also separates the zwitterions more, when no interaction between them is assumed. The interactions will draw them closer together, which, however, induces tensile forces due to the entropic spring nature of the chain between two covalent cross-links. As the swelling lengthens the distance between the cross-linkers, while the length of the chain stays constant, the entropic spring becomes stiffer; i.e., the zwitterions need to be pulled out of their position toward the other zwitterions with a

higher force. This effectively leads to less zwitterion–zwitterion interactions.

The hydrogel containing only pNIPAM self-evidently does not show these additional interactions and, hence, shows a Fickian diffusion behavior. In the absence of any relaxation within the frequency range of the experiment, the phase angle  $\delta(\omega)$  is very low ( $\approx 1^\circ$ ) and almost independent of swelling time. The modulus and the elongation at break  $\epsilon_H^{\max}$  are in the typical range of pNIPAM hydrogels.<sup>39–42</sup>

When considering the hydrogels containing pNIPAM and CNT, the stiffness is distinctly increased for 0.5% CNT but decreased for 1%. At the same time, the elongation at break  $\epsilon_H^{\max}$  increases slightly. This behavior can be attributed to CNTs bridging the microcracks and, thus, delaying crack propagation. Furthermore, the FESEM images show a thickening of the CNTs, which indicates that a significant amount of polymer is adsorbed on the CNTs. This adsorption depletes the network and, hence, effectively lowers the concentration of chains in the material, which are rheologically active; i.e., they contribute to the polymeric network. The dynamic-mechanical data show a slow relaxation process at low frequency, which is related to the adsorbed pNIPAM interacting with the CNT. The most likely explanation is a motion of chain segments on the CNT surface.

The swelling of these samples is unchanged in relation to the normal pNIPAM hydrogel in terms of mechanism. The maximum swelling, however, is significantly increased.

The addition of Zw to the hydrogels containing pNIPAM and CNT significantly increases the stiffness, while simultaneously significantly decreasing the elongation at break.  $\epsilon_H^{\max}$  of CNT0.5-Zw10 is smaller than that of both Zw10 and CNT0.5. When comparing the shear rheological data with the other samples, the phase angle  $\delta(\omega)$  is lower than that of the other samples (CNT0.5-Zw0 and CNT0-Zw10) and is almost time independent, indicating that although the water content increases by a factor of 7% throughout the experiment, the structure remains almost unchanged. This greatly decreased phase compared to the hydrogels containing either CNT or Zw suggests an interaction between these two components.

Previous results indicate<sup>51,52</sup> that the zwitterions can form a stable shell around CNT, which means that in the NIPAM, CNT, and Zw hydrogels the zwitterions “cross-link supramolecularly” the CNT with the polymeric network. As this interaction is rather stable, the phase angle  $\delta$  is reduced to almost the level of the pure pNIPAM-gel (CNT0-Zw0). For CNT0.5-Zw10,  $\delta(\omega)$  is slightly increased at the lowest frequencies, indicating that the zwitterion content is too low to fully suppress the CNT relaxation at low  $\omega$ , while CNT0.5-Zw20 has an upturn of  $\delta(\omega)$  at high  $\omega$ , which can be attributed to an excessively high zwitterion content in relation to the CNT content; i.e., the surface of the CNT is too small for the amount of Zw in the sample.

The mechanism of the interaction between Zw and CNT (“encapsulation”) also rationalizes the finding that the diffusion mechanism in NIPAM, CNT, and Zw hydrogels are Fickian, as these two groups form a stable complex, which does not change its properties, throughout the swelling.

The fact that in both dynamic-mechanical properties and in swelling properties, the Zw become “invisible” by complexing the CNTs as they attach themselves to the surface also explains why the stiffness is significantly higher and the elongation at break  $\epsilon_H^{\max}$  is very low. The CNTs are mechanically well integrated into the hydrogel network by their attraction of a

significant fraction of the Zw groups. For this reason, their influence on the mechanical behavior is comparable to that of fiber composites, while for the sample without Zw, the CNTs are much less strongly bound to the network, which renders the gel softer and more flexible. The FESEM images confirm this finding by showing significantly higher CNT thicknesses than the initial thickness of the unreacted CNTs, which indicates that the CNT surface is covered by zwitterions and the adjacent pNIPAM chains.

This is further evidence that CNTs can be trapped within the hydrogel by zwitterions in the polymeric network, which reduces the likelihood of CNTs being washed out of the hydrogel and potentially harming the environment.

## SUMMARY

The diffusion mechanisms in pNIPAM-based hydrogels were proven to be tailorable by the addition of zwitterions and CNTs. Supramolecularly cross-linked zwitterions lead to a very anomalous three-stage behavior: delayed initial diffusion, rapid anomalous non-Fickian diffusion, followed by normal Fickian diffusion. While the first two stages are dominated by the zwitterions first delaying but then speeding up the diffusion, the diffusion in the final stage is determined by the pNIPAM network.

While CNT has almost no influence on the diffusion itself, its capability to adsorb Zw on the surface changes the diffusion mechanism in the hydrogels that contain both components.

The change of the properties of the hydrogels in terms of diffusion mechanism, and shear and elongational rheology, as well as the structure observed by FESEM, confirms the supramolecular interaction between CNT and Zw, which affords a new property profile that can be used in various fields such as sensor, actuator, and biomedical applications.<sup>53,54</sup>

## ASSOCIATED CONTENT

### Supporting Information

Figures S1 and S2. This material is available free of charge via the Internet at <http://pubs.acs.org>.

## AUTHOR INFORMATION

### Corresponding Author

\*(F.J.S.) E-mail [fjstadler@jbnu.ac.kr](mailto:fjstadler@jbnu.ac.kr); Ph +82-63-270-4039; Fax +82-63-270-2306. (M.V.) E-mail: [mvatankhah@aut.ac.ir](mailto:mvatankhah@aut.ac.ir).

### Notes

The authors declare no competing financial interest.

## ACKNOWLEDGMENTS

The authors acknowledge the financial aid from the National Research Foundation of Korea (“Synthesis and Characterization of Intelligent Self-Healing Double-Network Hydrogels”) and “Human Resource Development (Advanced track for Si-based solar cell materials and devices, project number 201040100660)” of the Korean Institute of Energy Technology Evaluation and Planning (KETEP) grant funded by the Korea government Ministry of Knowledge Economy. F.O. would like to thank Chonbuk National University for the financial support. The authors thank the staff of the CBNU central lab for help with the FESEM images. The authors also thank Mr. Hyun Geun Ock and Prof. Dr. Ahn Kyung-hyun for help with SER measurements.

## REFERENCES

- (1) Chen, J.; Hamon, M. A.; Hu, H.; Chen, Y. S.; Rao, A. M.; Eklund, P. C.; Haddon, R. C. *Science* **1998**, 282 (5386), 95–98.
- (2) O'Connell, M. J.; Boul, P.; Ericson, L. M.; Huffman, C.; Wang, Y. H.; Haroz, E.; Kuper, C.; Tour, J.; Ausman, K. D.; Smalley, R. E. *Chem. Phys. Lett.* **2001**, 342 (3–4), 265–271.
- (3) Yu, M. F.; Lourie, O.; Dyer, M. J.; Moloni, K.; Kelly, T. F.; Ruoff, R. S. *Science* **2000**, 287 (5453), 637–640.
- (4) Xia, Y.; Yin, X. C.; Burke, N. A. D.; Stover, H. D. H. *Macromolecules* **2005**, 38 (14), 5937–5943.
- (5) Douglas, T. A.; Tamburro, D.; Fredolini, C.; Espina, B. H.; Lepene, B. S.; Ilag, L.; Espina, V.; Petricoin, E. F.; Liotta, L. A.; Luchini, A. *Biomaterials* **2011**, 32 (4), 1157–1166.
- (6) Wang, D.; Liu, T.; Yin, J.; Liu, S. Y. *Macromolecules* **2011**, 44 (7), 2282–2290.
- (7) Saleem, Q.; Liu, B. X.; Gradinaru, C. C.; Macdonald, P. M. *Biomacromolecules* **2011**, 12 (6), 2364–2374.
- (8) Ma, X. M.; Huang, X. B.; Zhu, L.; Zhao, X.; Tang, X. Z. *Polym. Int.* **2005**, 54 (1), 83–89.
- (9) Gholap, S. G.; Badiger, M. V. *J. Appl. Polym. Sci.* **2004**, 93 (3), 1454–1461.
- (10) Lynch, I.; Dawson, K. A. *J. Phys. Chem. B* **2004**, 108 (30), 10893–10898.
- (11) Shi, J. H.; Guo, Z. X.; Zhan, B. H.; Luo, H. X.; Li, Y. F.; Zhu, D. B. *J. Phys. Chem. B* **2005**, 109 (31), 14789–14791.
- (12) Isik, B. *Adv. Polym. Technol.* **2003**, 22 (3), 246–251.
- (13) Annaka, M.; Matsuura, T.; Kasai, M.; Nakahira, T.; Hara, Y.; Okano, T. *Biomacromolecules* **2003**, 4 (2), 395–403.
- (14) Haraguchi, K.; Takada, T. *Macromol. Chem. Phys.* **2005**, 206 (15), 1530–1540.
- (15) Kuckling, D.; Harmon, M. E.; Frank, C. W. *Macromolecules* **2002**, 35 (16), 6377–6383.
- (16) Zha, L. S.; Hu, J. H.; Wang, C. C.; Fu, S. K.; Luo, M. F. *Colloid Polym. Sci.* **2002**, 280 (12), 1116–1121.
- (17) Collins, M. N.; Birkinshaw, C. *J. Mater. Sci.: Mater. Med.* **2008**, 19 (11), 3335–43.
- (18) Yildiz, B.; Isik, B.; Kis, M. *React. Funct. Polym.* **2002**, 52 (1), 3–10.
- (19) Garcia-Salinas, M. J.; Romero-Cano, M. S.; de las Nieves, F. J. *J. Colloid Interface Sci.* **2001**, 241 (1), 280–285.
- (20) Yildiz, B.; Isik, B.; Kis, M. *Eur. Polym. J.* **2002**, 38 (7), 1343–1347.
- (21) Gan, D. J.; Lyon, L. A. *J. Am. Chem. Soc.* **2001**, 123 (34), 8203–8209.
- (22) Jones, C. D.; Lyon, L. A. *Macromolecules* **2000**, 33 (22), 8301–8306.
- (23) Xiao, X. C.; Chu, L. Y.; Chen, W. M.; Wang, S.; Xie, R. *Langmuir* **2004**, 20 (13), 5247–5253.
- (24) Lee, W.-F.; Yeh, P.-L. *J. Appl. Polym. Sci.* **1999**, 74, 2170–2180.
- (25) Isik, B.; Gunay, Y. *Colloid Polym. Sci.* **2004**, 282 (7), 693–698.
- (26) Akdemir, Z. S.; Kayaman-Apohan, N. *Polym. Adv. Technol.* **2007**, 18 (11), 932–939.
- (27) Zhang, L. M.; Hu, Z. H. *Starch/Starke* **2002**, 54 (7), 290–295.
- (28) Paris, R.; Barrales-Rienda, J. M.; Quijada-Garrido, I. *Polymer* **2009**, 50 (9), 2065–2074.
- (29) Patel, M. P.; Johnstone, M. B.; Hughes, F. J.; Braden, M. *Biomaterials* **2001**, 22 (1), 81–86.
- (30) Cai, W. S.; Gupta, R. B. *J. Appl. Polym. Sci.* **2003**, 88 (8), 2032–2037.
- (31) Ritger, P. L.; Peppas, N. A. *J. Controlled Release* **1987**, 5, 37–42.
- (32) Ritger, P. L.; Peppas, N. A. *J. Controlled Release* **1987**, 5, 23–36.
- (33) Mullarney, M. P.; Seery, T. A. P.; Weiss, R. A. *Polymer* **2006**, 47 (11), 3845–3855.
- (34) Frisch, H. L. *Polym. Eng. Sci.* **1980**, 20 (1), 2–13.
- (35) Wasaki, K.; Kajihara, T.; Kawashima, T.; Nagano, H.; Nakashima, S. Method for production of alkylamino(Meth)acrylate and apparatus therefor. US Patent 6417392, 2002.
- (36) Grunlan, J. C.; Liu, L.; Kim, Y. S. *Nano Lett.* **2006**, 6 (5), 911–915.
- (37) Hashmi, S.; Obiweleozor, F.; GhavamiNejad, A.; Vatankhah-Varnoosfaderani, M.; Stadler, F. J. *Korea-Australia Rheol. J.* **2012**, 24 (3), 191–198.
- (38) Hencky, H. Z. *Tech. Phys.* **1928**, 9, 215–220.
- (39) Stadler, F. J.; Friedrich, T.; Tieke, B.; Bailly, C. *Rheol. Acta* **2013**, submitted.
- (40) Friedrich, T.; Tieke, B.; Stadler, F. J.; Bailly, C. *Langmuir* **2011**, 27, 2997–3005.
- (41) Friedrich, T.; Tieke, B.; Stadler, F. J.; Bailly, C. *Macromolecules* **2010**, 43 (23), 9964–9971.
- (42) Friedrich, T.; Tieke, B.; Stadler, F. J.; Bailly, C. *Soft Matter* **2011**, 7 (14), 6590–6597.
- (43) Stadler, F. J. *Rheol. Acta* **2010**, 49 (10), 1041–1057.
- (44) Chattopadhyay, D.; Lastella, S.; Kim, S.; Papadimitrakopoulos, F. *J. Am. Chem. Soc.* **2002**, 124 (5), 728–729.
- (45) Lowe, A. B.; McCormick, C. L. *Chem. Rev.* **2002**, 102 (11), 4177–4189.
- (46) Stadler, F. J.; Bailly, C. *Rheol. Acta* **2009**, 48 (1), 33–49.
- (47) Lee, W. F.; Chen, C. F. *J. Appl. Polym. Sci.* **1998**, 69 (10), 2021–2034.
- (48) Macosko, C. W. *Rheology: Principles, Measurements and Applications*; Wiley/VCH: Poughkeepsie, NY, 1994.
- (49) Trouton, F. T. *Proc. R. Soc. London* **1906**, 77, 426.
- (50) Stadler, F. J.; Münstedt, H. *Macromol. Mater. Eng.* **2009**, 294 (1), 25–34.
- (51) Soll, S.; Antonietti, M.; Yuan, J. Y. *ACS Macro Lett.* **2012**, 1 (1), 84–87.
- (52) Zhang, W.; Swager, T. M. *J. Am. Chem. Soc.* **2007**, 129 (25), 7714–+.
- (53) Chang, Y.; Yandi, W.; Chen, W. Y.; Shih, Y. J.; Yang, C. C.; Chang, Y.; Ling, Q. D.; Higuchi, A. *Biomacromolecules* **2010**, 11 (4), 1101–1110.
- (54) Chaterji, S.; Kwon, I. K.; Park, K. *Prog. Polym. Sci.* **2007**, 32 (8–9), 1083–1122.